Frank Schellenberger, Noemí Encinas, Doris Vollmer, Hans-Jürgen Butt
Phys. Rev. Lett. (2016), 116, 096101

How water advances on superhydrophobic surfaces

Authors: Frank Schellenberger, Noemí Encinas, Doris Vollmer, Hans-Jürgen Butt*

Affiliation:

Max Planck Institute for Polymer Research, Ackermannweg 10, 55128 Mainz, Germany

*Correspondence to: butt@mpip-mainz.mpg.de

Keywords: Superamphiphobic, superoleophobic, superomniphobic, Cassie-Baxter equation, tilted plane

Super liquid-repellency can be achieved by nano- and microstructuring surfaces in such a way, that protrusions entrap air underneath the liquid. It is still not known, how the three-phase contact line advances on such structured surfaces. In contrast to a smooth surface, where the contact line can advance continuously, on a super liquid-repellent surface the contact line has to overcome an air gap between protrusions. Here, we apply laser scanning confocal microscopy to get the first microscopic videos of water drops advancing on a superhydrophobic array of micropillars. In contrast to common belief, the liquid surface gradually bends down until it touches the top face of the next micropillars. The apparent advancing contact angle is 180°. On the receding side, pinning to the top faces of the micropillars determines the apparent receding contact angle. Based on these observations, we propose that the apparent receding contact angle should be used for characterizing super liquid-repellent surfaces, rather than the apparent advancing contact angle and hysteresis.

Research on the wetting of micro- and nanostructured surfaces is motivated by the challenge to control wetting, in particular to fabricate surfaces which repel liquids. Super liquid-repellent surfaces are for example self-cleaning [1], can reduce hydrodynamic drag [2] are used for fog harvesting [3, 4], enhancing heat transfer [5], and gas exchange [6]. One strategy to achieve super liquid-repellency is to structure low-energy surfaces on the nano- and micrometer length scale. This structure needs to be such that protrusions keep the drop from direct contact with the substrate. A layer of air is maintained underneath the drop leading to the so-called Cassie or Fakir state [7-13]. Only the top faces of the protrusions are in direct contact with the liquid. In contrast, when the liquid wets the surface without trapping air, in the so-called Wenzel state, super liquid-repellency is lost.

For an understanding of the wetting behavior of drops on super liquid-repellent surfaces, most progress has been made using superhydrophobic micropillar arrays [8, 14-16]. One of the open questions is: How does a drop advance on a superhydrophobic surface? First insight into the microscopic process was obtained by recent theoretical studies using Surface Evolver [17] or energy minimizations [18]. For modeling advancing drops these methods are, however, restricted to the Wenzel state. From the experimental side, in by far most publications on superhydrophobic surfaces, apparent receding contact angles above 150° and advancing contact angles below 170° were reported (Table S1, supporting information). Hardly without any exception, apparent contact angles are measured using a goniometer in combination with a video camera and drop shape analysis. However, measuring contact angles above 150° is difficult. For high contact angles the narrow gap between the liquid and the solid makes it hard to identify the position of the contact line [19-21] and drop vibrations can change the result [22]. Bartell, Shepard, Extrand, Gao, and McCarthy speculated that the advancing contact angle could take 180° [20, 23, 24]. To our knowledge, no simulation or measurement exist, confirming or falsifying this hypothesis.

Progress in our understanding of the intimate relationship between nano- and microstructure and macroscopic wetting phenomena has been hampered by the lack of microscopic images of advancing drops. Using scanning electron microscopy [25-27] and confocal microscopy [28] the contact lines of static drops have been imaged with a resolution better than 1 µm. However, the process of a moving contact line and in particular the limiting case, the contact angle just before advancing, has never been imaged.

Here, we used an inverted laser scanning confocal microscope to image the advancing and receding side of water drops sliding on superhydrophobic micropillar arrays. To let drops move, we carefully tilted the vibration isolation table onto which the microscope was mounted by hand with a hydraulic car jack. The inclination angle was measured with an optical beam. After recording confocal microscope videos they were further processed (Fig. S1, supporting information SI). Superhydrophobic arrays of cylindrical micropillars with flat top faces were fabricated as described in [28] (Fig. 1 and SI). Three different square arrays of epoxy-based SU-8 with pillar diameters a and pillar spacings b of 5 and 15 µm, 10 and 30 µm,

25 and 75 µm, respectively, were investigated. The area fraction, $f = \pi a^2 / 4(a+b)^2 = 0.049$, was kept constant. Pillars were 9-16 µm high. Apparent advancing and receding contact angles measured with a goniometer (Dataphysics OCA35) using the sessile drop method (3-5 µL water drops) were Θ_a^{app}=165±3° and Θ_r^{app}=142±5°, respectively. The contact angles of water on an equally treated flat SU-8 surface after coating with a silica layer and hydrophobization were Θ_a=124°±2° (advancing) and Θ_r=85°±5° (receding). Errors were derived from repeated measurements with different samples. Within experimental resolution we did not observe different apparent contact angles on the different geometries.

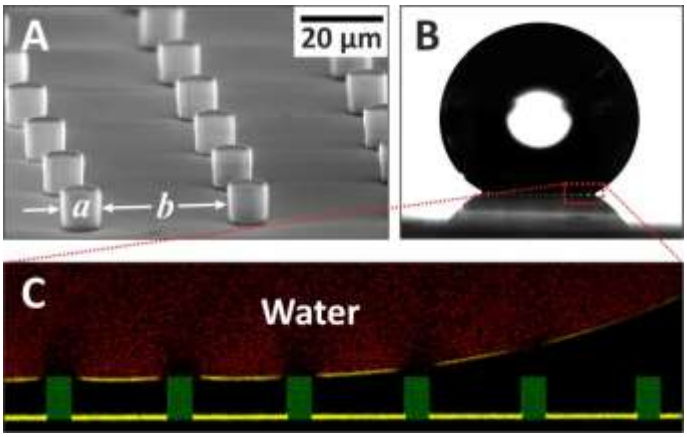

FIG. 1. **A**: Scanning electron micrograph of an array of the cylindrical micropillars. Diameter and micropillar distance are indicated by *a* and *b*, respectively. The microstructure consists of SU-8 coated with a 70 nm thick layer of silica and hydrophobized with (1H,1H,2H,2H)-per-fluorooctyl-trichlorosilane via chemical vapor deposition. **B**: Contour of a 2 mm high water drop on a micropillar array. **C**: Confocal microscope vertical images of a water drop on a superhydrophobic micropillar surface (pillar diameter *a*=10 µm, pillar distance *b*=30 µm, height *h*=15 µm). We used an inverted confocal microscope (Leica TCS SP8 SMD, HCX PL APO 40× dry objective) with a resolution of about 0.25 µm and 1.0 µm in the horizontal and vertical direction, respectively. Millipore water was fluorescently dyed with Alexa Fluor 488 at a concentration of 1 µg/mL. The fluorescence of Alexa in water is shown in red. The surface tension as measured with the pendant drop method was 72.8±0.2 mN/m; within this error it did not change when adding Alexa. Reflection and emission signals were recorded simultaneously. Care was taken to ensure that the vertical sections of the imaging plane passed through the centre of the drop. After recording confocal microscope videos they were further processed (Fig. S1, SI). The water-air (top yellow line) and substrate-air interfaces (bottom horizontal yellow line) are imaged in reflection. The interruptions in the yellow water-air interface are due to optical artifacts, as explained in Fig. S1. The pillars (green) are simulated.

In the literature a number of definitions for contact angles are discussed [18, 29, 30]. We define the “apparent” advancing contact angle as the slope of the drop’s surface at the

horizontal going through the top faces of the micropillars. The surface of the drop, determined with optical resolution (≈1 µm), was extrapolated to the horizontal plane. “Advancing” indicates that this procedure is carried out on the advancing side of the drop just before it actually starts sliding. In this situation the drop is still static.

An experiment started by carefully placing a water drop of 5±1 µL volume on the superhydrophobic surface. Then we gradually tilt the surface in the direction of one of the axes of the array. The drop distorts. At some inclination the contact line starts to shift and the apparent contact area becomes more elliptical. When the inclination reaches the roll-off angle of α = 9°±1° we typically observe an induction period. After typically 30 s the drop will start rolling off the surface.

When imaging the advancing front in the induction period with the confocal microscope we observed that the contact line does not jump from one pillar to the next. Rather, sections of the liquid-vapor interface descend onto the top face of the next micropillar (Fig. 2, Video 1 SI). One representative sequence of a drop which is going to move to the right is shown in Figure 2. The temporary contact angle increased from 174° until it reached almost 180°. The top face of the next pillar was wetted after 7.6 s (Fig. 2B). Contact with the next micropillars was established after 10.9, 13.6, 16.7, 20.9, 23.5, and 26.4 s. Following the definition of e.g. Semprebon et al. [18] the maximal, static apparent contact angle on the advancing front was Θ_a^{app}=180°. Thus, our observations verify the scenario proposed by Bartell, Shepard, Extrand, Gao, and McCarthy [20, 23, 24]. After 27 s the drop started its fast descent downhill. From the passing of the rear of the drop through the field of view a rolling velocity of the order of 1 mm/s could be estimated.

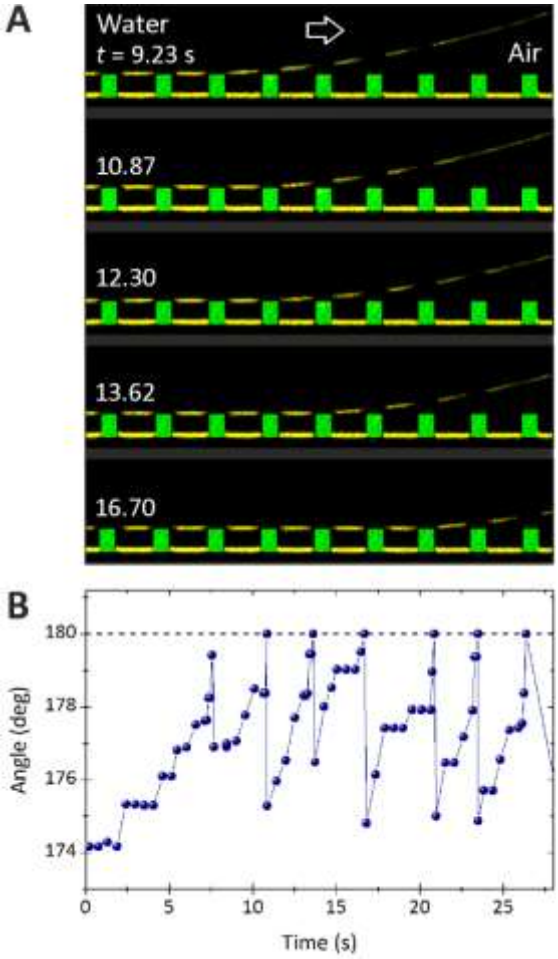

FIG. 2: Advancing water front on a superhydrophobic micropillar array. (A) Confocal vertical images of the advancing front of a water drop on a superhydrophobic micropillar surface (pillar diameter a=5 µm, pillar distance b=15 µm, height h=9 µm) before the drop starts rolling. The inclination of 9° was kept constant. The water-air (top yellow line) and substrate-air interfaces (bottom horizontal yellow line) are imaged in reflection. The pillars (green) are simulated. (B) Advancing contact angles measured from confocal images plotted versus time. How contact angles were determined is shown in Figure S2.

Figure 2 was recorded on an array with a micropillar spacing of b=15 µm. When using arrays with a larger dimension (a=10 µm, b=30 µm) the water surface even bulged below the horizontal plane (Fig. 3 A+B, Video 2). Figure 3A shows a sequence of three representative confocal images. At t = 13.33 s the water front has just touched on the third pillar from the left. The water surface then gradually bends downwards, exceeds an angle of 180° at t = 24 s, reaches an angle of 183° at t = 29.74 s and afterwards touches the top face of the next pillar. Thus, at t = 29.85 s the angle needs to be counted from the fourth pillar from the left. The moment when the water front touches the top face of the next pillar can again be clearly defined because the reflection due to the air gap observed in the unfiltered images

disappears (unfiltered insets in Fig. 3A). The insets in Figure 3A show the 4th and 5th micropillar from the left.

On arrays with the largest dimensions (a=25 µm, b=75 µm) the angle on the advancing side even approached 188° until the next micropillar was wetted (Video 3, Fig. 3C,D). Angles above 180° reflect the fact that the liquid surface has a curvature, which is determined by the drop size via the Laplace equation. This curvature is also observed between all pillars in the contact region.

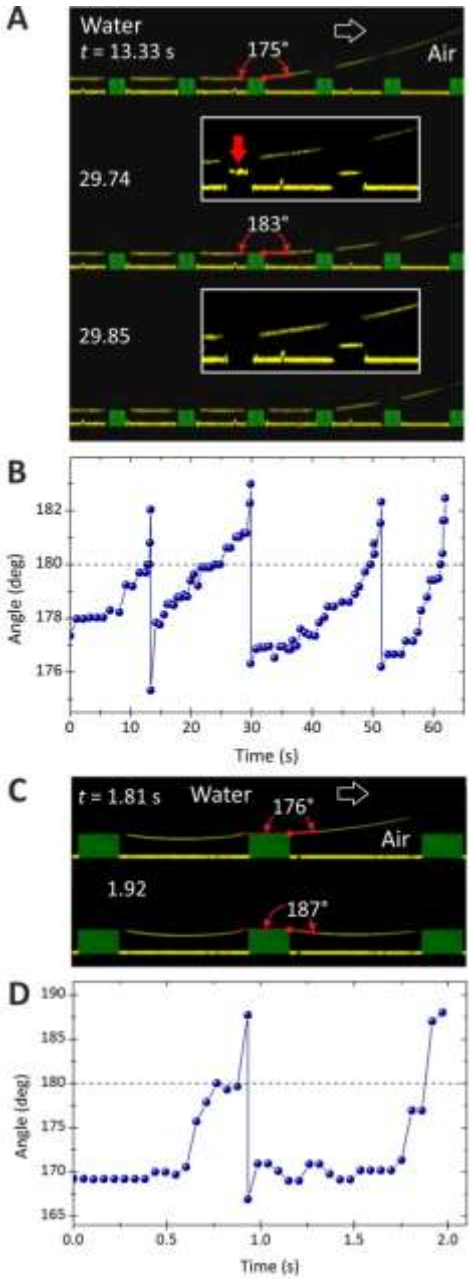

FIG. 3: Water front advancing on a superhydrophobic micropillar array. (A) Confocal vertical images of a water drop just before advancing on a superhydrophobic micropillar surface (pillar diameter a=10 µm, distance b=30 µm, height h=10 µm). The inclination at the roll-off angle of 9° was kept constant. The water-air (top yellow line) and substrate-air-interfaces (bottom horizontal yellow line) are imaged in reflection. Insets show unfiltered

details containing the 4th and 5th micropillar from the left. The reflex indicated by a red arrow indicates the air gap between the drop and the top face of the 4th micropillar. (B) Angles measured from confocal images plotted versus time. The results were obtained from video 2. (C) A water drop just before advancing on a superhydrophobic micropillar surface with a=25 µm, b=75 µm, and h=14 µm. The inclination at the roll-off angle of 8.5° was kept constant. D) Angles measured from confocal images plotted versus time. The results were obtained from video 3.

With increasing micropillars spacing and in particular for arrays with the largest dimensions (a=25 µm, b=75 µm) recording images was more difficult. The descent of the liquid front onto the top face of the next pillar was faster and it was more difficult to record intermediate stages. The decreased stability was most likely the combination of two effects. First, when the drop changes the apparent contact area, it detaches from individual micropillars at the rear side. These detachments causes capillary vibrations. Their amplitude increase with increasing micropillar spacing. Second, the wavelength of vibrations at the rim is limited by the micropillar spacing. Since the maximal restoring pressure of the drop at the rim also increases with decreasing micropillar spacing, smaller micropillar spacing leads to smaller vibration amplitudes (SI).

In contrast to the advancing side, on the rear side of drops (Fig. 4, Video 4) we observed a discontinuous movement. The contact line is pinned until a certain lower critical contact angle, Θ_r^{app}, is reached. Then the liquid front jumps to the next pillar. Since Θ_r^{app} is the maximal stable apparent contact angle on the rear side of the drop, this angle is the apparent receding contact angle. For practical reasons we measured the apparent contact angle at a height of 10 µm above the pillars top faces and not directly at the height of the top faces (indicated in figure 4 at t=31.76 s). Reason: The curvature of liquid bridges directly at the top faces of the micropillars in the contour plane was relatively high. At a height of 10 µm the error in determining the slope of the drop shape was lower. In this way the apparent receding contact angle is to a certain degree arbitrary. The discontinuous movement and the fact that there is a lower critical angle is, however, consistent. The apparent receding contact angle observed with the goniometer (Θ_r^{app}=142±5°) agrees with values recorded with the confocal microscope (Θ_r^{app}=140±3°).

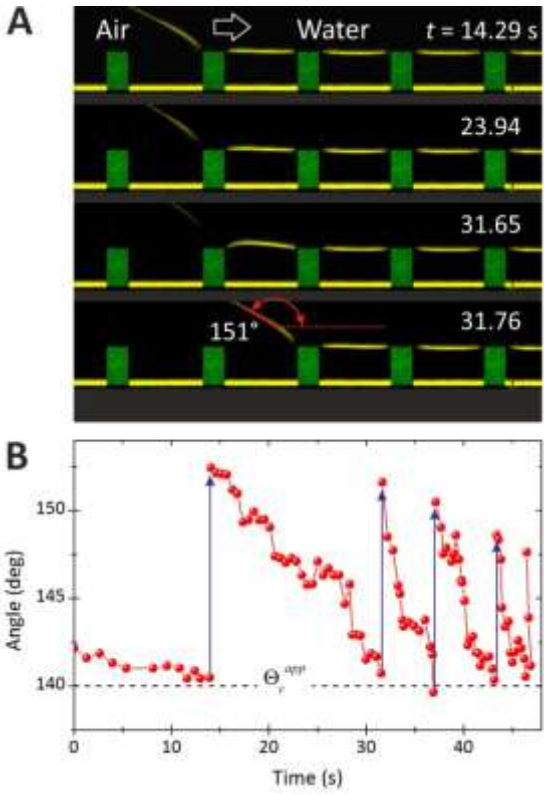

FIG. 4: Receding water front on a superhydrophobic micropillar array. (A) Confocal vertical cross section of the receding side of a water drop moving to the right on a superhydrophobic micropillar array (a=10 µm, b=30 µm, h=16 µm). The inclination of 9° was kept constant. The rear side detaches from the pillars at 14.3, 31.8, 37.3, 43.5 s. After 46.6 s the drop gets out of the field of view and started its fast slide downhill. The water-air and substrate-air interfaces (yellow) are imaged in reflection. The dark blue arrows indicate jumps of the contact line. (B) Receding angles measured from confocal images plotted versus time.

These observations have several implications:

- A surface is commonly defined "superhydrophobic" when the apparent advancing contact angle of water exceeds 150° and when the hysteresis $\Delta\Theta = \Theta_a^{app} - \Theta_r^{app}$ is lower than 10°. Both values are almost exclusively measured with a goniometer. Sometimes the second condition is replaced by demanding a low roll-off angle. Confocal microscope images demonstrate that the apparent advancing contact angle measured with a goniometer may be significantly underestimated. It depends on the way the drop is placed on the surface and external vibrations rather than intrinsic properties of the surface. We measured 165° with the goniometer but the real advancing contact angle on micropillars with flat top faces was $\Theta_a{}^{app}$=180°. This implies that apparent advancing contact angles are not suitable to characterize super-liquid repellent surfaces. In fact, apparent advancing contact angles close to 180° or even larger may even be characteristic for superhydrophobic surfaces.

- Underestimating Θ_a^{app} in goniometer measurements also implies that $\Delta\Theta$ is underestimated. Therefore, superhydrophobicity cannot be defined by a low contact angle hysteresis.
- In general, a drop rolls off an inclined surface when the tilt angle α exceeds a value given by [15, 31-33]

$$\sin\alpha = \frac{k\gamma w}{V\rho g}\left(\cos\Theta_r^{app} - \cos\Theta_a^{app}\right) \tag{1}$$

  Here, γ is the surface tension of the liquid, w is the width of the apparent contact area measured perpendicular to the sliding direction, V is the volume of the drop, ρ is the density of the liquid, g=9.81 m/s^2 is the acceleration of gravity, and $k\approx1$ is a geometry factor. Eq. (1) is the results of a force balance between gravitation pulling the drop downhill and the capillary force, i.e. the integral of surface tension around the contact line of the drop. Eq. (1) is also valid for super liquid-repellent surfaces as long as the drop is much larger than the spacing between protrusions. Our results show that for many if not all superhydrophobic surfaces $\Theta_a^{app}\approx180°$ and Eq. (1) simplifies:

$$\sin\alpha = \frac{k\gamma w}{V\rho g}\left(\cos\Theta_r^{app} + 1\right) \tag{2}$$

- To design superhydrophobic surfaces and calculate apparent contact angles usually the Cassie-Baxter theory is applied [7]. It is based on minimization of the global Gibbs free energy. For a comparison with experiments, the equilibrium contact angle is often set equal to the apparent advancing contact angle [8], which leads to [7-9]

$$\cos\Theta_a^{app} = f\left(\cos\Theta + 1\right) - 1 \tag{3}$$

  Here, Θ is the Young or materials contact angle as measured on a smooth, planar surface of the same material. It was later clarified that the surface fractions local to the drop perimeter need to be inserted [10-13]. Our observations demonstrate that the Cassie-Baxter equation is not suitable to describe the apparent advancing contact angle. It does not reflect the underlying physical process. Also the predictions of Eq. (3) are erroneous. In our case, f = 4.9% and Θ_a = 124° leads to a predicted Θ_a^{app} of 168° and not 180°.

- We propose that for the definition of superhydrophobicity the apparent receding contact angle is used. A surface should be called “superhydrophobic” if the apparent receding contact angle exceeds a certain value, e.g. 150°. A high apparent receding contact angle is inherently connected to a low roll-off angle but has the advantage of being independent on drop size [21].

All super liquid-repellent surfaces, including surfaces which repel non-polar liquids or solutions with surface active agents (superoleophobic, -amphiphobic or –omniphobic surfaces) rely on protrusions to establish the Cassie state. Therefore, micropillar arrays are a good model and we expect the conclusions to be valid for all super liquid-repellent surfaces.

Acknowledgments: We thank Tadashi Kajiya, Nan Gao, Sanghyuk Wooh, Periklis Papadopoulos for helpful discussions. Financial support from ERC grant SuPro (H.J.B.), COST1106 (D.V.) and the Marie Skłodowska-Curie fellowship 660523-NoBios-ESR (N.E.) are acknowledged.

[1] W. Barthlott, and C. Neinhuis, Planta **202**, 1 (1997).

[2] J. P. Rothstein, Annu. Rev. Fluid Mech. **42**, 89 (2010).

[3] Y. M. Zheng, H. Bai, Z. B. Huang, X. L. Tian, F. Q. Nie, Y. Zhao, J. Zhai, and L. Jiang, Nature **463**, 640 (2010).

[4] K. C. Park, S. S. Chhatre, S. Srinivasan, R. E. Cohen, and G. H. McKinley, Langmuir **29**, 13269 (2013).

[5] N. Miljkovic, and E. N. Wang, MRS Bulletin **38**, 397 (2013).

[6] M. Paven, P. Papadopoulos, S. Schöttler, X. Deng, V. Mailänder, D. Vollmer, and H.-J. Butt, Nature Commun. **4**, 2512 (2013).

[7] A. B. D. Cassie, and S. Baxter, Trans. Faraday Soc. **40**, 546 (1944).

[8] J. Bico, C. Marzolin, and D. Quéré, Europhys. Lett. **47**, 220 (1999).

[9] A. Marmur, Langmuir **19**, 8343 (2003).

[10] G. McHale, Langmuir **23**, 8200 (2007).

[11] M. Nosonovsky, Langmuir **23**, 9919 (2007).

[12] W. Choi, A. Tuteja, J. M. Mabry, R. E. Cohen, and G. H. McKinley, J. Colloid Interface Sci. **339**, 208 (2009).

[13] H. Y. Erbil, Surf. Sci. Rep. **69**, 325 (2014).

[14] D. Öner, and T. J. McCarthy, Langmuir **16**, 7777 (2000).

[15] Z. Yoshimitsu, A. Nakajima, T. Watanabe, and K. Hashimoto, Langmuir **18**, 5818 (2002).

[16] C. Priest, T. W. J. Albrecht, R. Sedev, and J. Ralston, Langmuir **25**, 5655 (2009).

[17] C. Dorrer, and J. Rühe, Langmuir **23**, 3179 (2007).

[18] C. Semprebon, S. Herminghaus, and M. Brinkmann, Soft Matter **8**, 6301 (2012).

[19] S. Srinivasan, G. H. McKinley, and R. E. Cohen, Langmuir **27**, 13582 (2011).

[20] L. Gao, and T. J. McCarthy, Langmuir **22**, 2966 (2006).

[21] J. T. Korhonen, T. Huhtamaki, O. Ikkala, and R. H. A. Ras, Langmuir **29**, 3858 (2013).

[22] E. Pierce, F. J. Carmona, and A. Amirfazli, Colloids & Surfaces A **323**, 73 (2008).

[23] F. E. Bartell, and J. W. Shepard, J. Phys. Chem. **57**, 455 (1953).

[24] C. W. Extrand, Langmuir **18**, 7991 (2002).

[25] Y. T. Cheng, D. E. Rodak, A. Angelopoulos, and T. Gacek, Appl. Phys. Lett. **87**, 194112 (2005).

[26] M. Nosonovsky, and B. Bhushan, Langmuir **24**, 1525 (2008).

[27] A. T. Paxson, and K. K. Varanasi, Nature commun. **4**, 1492 (2013).

[28] P. Papadopoulos, L. Mammen, X. Deng, D. Vollmer, and H. J. Butt, Proc. Natl. Acad. Sci. USA **110**, 3254 (2013).

[29] E. L. Decker, B. Frank, Y. Suo, and S. Garoff, Colloids & Surfaces A **156**, 177 (1999).

[30] K. G. Winkels, I. R. Peters, F. Evangelista, M. Riepen, A. Daerr, L. Limat, and J. H. Snoeijer, Eur. Phys. J. Special Topics **192**, 195 (2011).

[31] C. G. L. Furmidge, J. Colloid Sci. **17**, 309 (1962).

[32] A. ElSherbini, and A. Jacobi, J. Colloid Interface Sci. **299**, 841 (2006).

[33] C. Antonini, F. J. Carmona, E. Pierce, M. Marengo, and A. Amirfazli, Langmuir **25**, 6143 (2009).